PNAS RESEARCH ARTICLE | APPLIED PHYSICAL SCIENCES

T-linear resistivity from magneto-elastic scattering: Application to $PdCrO_2$

J. F. Mendez-Valderrama[a,1], Evyatar Tulipman[b,1], Elina Zhakina[c], Andrew P. Mackenzie[c,d], Erez Berg[b], and Debanjan Chowdhury[a,2]

Edited by Aharon Kapitulnik, Stanford University, Stanford, CA; received April 6, 2023; accepted July 5, 2023

An electronic solid with itinerant carriers and localized magnetic moments represents a paradigmatic strongly correlated system. The electrical transport properties associated with the itinerant carriers, as they scatter off these local moments, have been scrutinized across a number of materials. Here, we analyze the transport characteristics associated with ultraclean $PdCrO_2$—a quasi-two-dimensional material consisting of alternating layers of itinerant Pd-electrons and Mott-insulating CrO_2 layers—which shows a pronounced regime of T-linear resistivity over a wide range of intermediate temperatures. By contrasting these observations to the transport properties in a closely related material $PdCoO_2$, where the CoO_2 layers are band-insulators, we can rule out the traditional electron–phonon interactions as being responsible for this interesting regime. We propose a previously ignored electron-magneto-elastic interaction between the Pd-electrons, the Cr local moments and an out-of-plane phonon as the main scattering mechanism that leads to the significant enhancement of resistivity and a T-linear regime in $PdCrO_2$ at temperatures far in excess of the magnetic ordering temperature. We suggest a number of future experiments to confirm this picture in $PdCrO_2$ as well as other layered metallic/Mott-insulating materials.

electrical transport | Planckian scattering | Kondo materials

Significance

Electrical transport in correlated metals, and specifically a resistivity that scales linearly with temperature accompanied by a universal Planckian scattering rate, has received intense scrutiny in recent years. It is rare to have a correlated material where the effects of electron–electron and electron–phonon interactions can be systematically disentangled and where starting from a microscopically realistic model one can arrive at a quantitatively accurate theory for electrical transport. Building on a wealth of experimental data for a quasi-two-dimensional, ultraclean material consisting of alternately stacked layers of metals and Mott insulators, we describe a mechanism involving electrons scattering off phonons and fluctuating local moments, that can completely account for the measured linear in temperature resistivity.

Recent years have witnessed a resurgence of interest in the microscopic origin of an electrical resistivity that scales linearly with temperature (1, 2) and exhibiting a Planckian scattering rate, $\Gamma = Ck_BT/\hbar$, where $C \sim O(1)$ coefficient (3–7). In conventional (simple) metals at room temperature, this phenomenology is readily understood as a consequence of electrons scattering off thermally excited phonons in their equipartition regime (8). On the other hand, numerous "correlated" materials belonging to the cuprate (6, 7, 9, 10), pnictide (11, 12), ruthenates (13–17), rare-earth (18), and moiré bilayers (5, 19) display Planckian scattering down to low temperatures, likely driven by purely electronic interactions and where a priori it is unclear whether phonons play an essential role (3, 20–22). It is challenging to disentangle the role of electron–electron and electron–phonon interactions on scattering lifetimes. It is quite natural to ask whether materials with a nearly identical phonon spectrum and distinct electronic spectra can lead to a distinct temperature dependence of their respective resistivities.

An Experimental Puzzle

The goal of this paper is to resolve a conundrum inspired by electrical transport measurements in two isostructural quasi-two-dimensional compounds with distinct electronic structures: $PdCoO_2$ and $PdCrO_2$. Their structural motif consists of alternately stacked layers of highly conducting Pd and insulating CoO_2/CrO_2 in a triangular lattice arrangement (24–28); see Fig. 1*A*. The phonon spectra for the two compounds are nearly identical; some of the differences arise from the distinct ionic masses (27–30), and recent analysis has also revealed that the unit cell of $PdCrO_2$ is slightly enlarged due to the presence of magnetic moments (31). On the other hand, their electronic spectra are different since the CrO_2 layers are Mott-insulating with the local moments interacting via antiferromagnetic (AFM) exchange interactions (25, 32), while the CoO_2 layers are nonmagnetic (24, 26, 33). The photoemission spectrum of $PdCrO_2$ contains prominent features, absent in $PdCoO_2$ (28, 34–36), that can be understood from an effective interlayer Kondo lattice model (28). The in-plane resistivities for the two compounds (23) are shown in Fig. 1*B*, respectively. The salient features are as follows: i) The magnitude of the resistivity for both compounds is small, suggesting that they are "good" metals with a long mean-free path. ii) $PdCrO_2$ is considerably more resistive than $PdCoO_2$ over a wide range of temperatures. iii) $PdCrO_2$ displays a prominent T-linear scaling

Author contributions: A.P.M., E.B., and D.C. designed research; J.F.M.-V. and E.T. performed research; J.F.M.-V., E.T., E.Z., A.P.M., E.B., and D.C. analyzed data; and J.F.M.-V., E.T., E.B., and D.C. wrote the paper.

The authors declare no competing interest.

This article is a PNAS Direct Submission.

[1]J.F.M.-V. and E.T. contributed equally to this work.

[2]To whom correspondence may be addressed. Email: debanjanchowdhury@cornell.edu.

This article contains supporting information online at https://www.pnas.org/lookup/suppl/doi:10.1073/pnas.2305609120/-/DCSupplemental.

Published August 28, 2023.

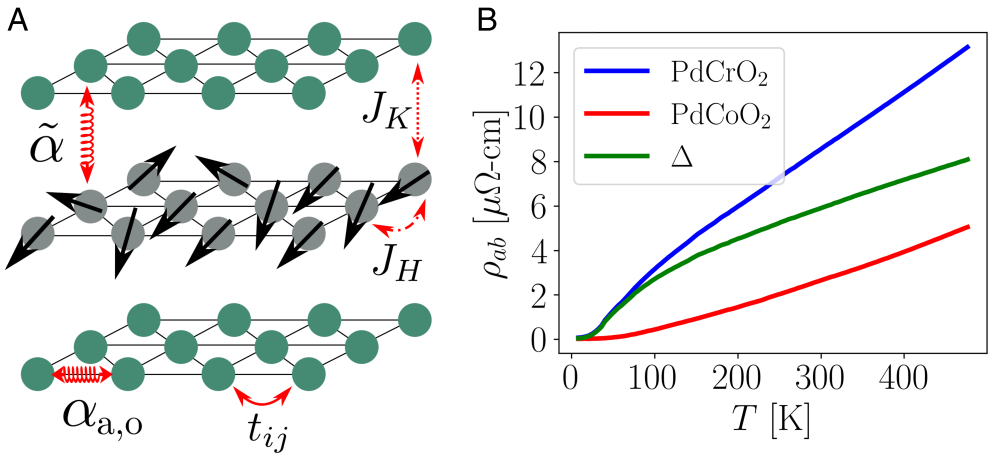

Fig. 1. (*A*) The structural motif in $PdCrO_2$, composed of alternating layers of triangular lattices of conducting Pd planes (green) and Mott insulating CrO_2 planes (gray). The different coupling constants denoted in the figure are as defined in Eq. **1a**. (*B*) The in-plane resistivities of $PdCrO_2$ and $PdCoO_2$ taken from ref. 23 along with their difference $\Delta\rho \equiv \rho_{ab}^{PdCrO_2} - \rho_{ab}^{PdCoO_2} > 0$.

of the resistivity above $T \gtrsim 150$ K (far above $T_N \approx 37.5$ K, the Néel temperature for 120°−antiferromagnetism) (25, 32, 37, 38), and with a slope that is greater than the average slope of $\rho_{ab}(T)$ in $PdCoO_2$ in the same temperature range (39).

The central puzzle that we address in this paper concerns the microscopic origin of the excess T-linear resistivity in $PdCrO_2$ relative to isostructural $PdCoO_2$ ($\Delta\rho \equiv \rho_{ab}^{PdCrO_2} - \rho_{ab}^{PdCoO_2} > 0$), going beyond the conventional electron–phonon scattering mechanism, and in a temperature regime where the long-range magnetic order is lost. Given the contrast between $PdCrO_2$ and $PdCoO_2$, it is plausible that the fluctuations of the Cr-local moments play a crucial role in the electronic transport lifetimes even at the relatively high temperatures of interest (i.e., for $T \gtrsim T_N$). However, recent work (40) has demonstrated that electrons scattering off the fluctuations of a "cooperative" paramagnet (41–48) can not account for a T-linear resistivity; instead, the resistivity saturates to a temperature-independent value for $T \gg T_N$. Starting with a microscopic model, we will now demonstrate that the resolution to the conundrum lies in a previously ignored and nontrivial interaction term between the Pd-electrons, the Cr-spins, and phonons, as encoded in an electron-magneto-elastic (EME) coupling. Although specifically motivated by $PdCrO_2$, our theory has relevance beyond this single material. There are a number of exciting new material platforms that have come to the forefront in recent years that consist of stacks of metallic and Mott insulating layers (49–57). In what follows, we develop a general framework to address electrical transport in such layered material platforms, and our conclusions can be used to disentangle the various sources of interaction between electrons, local moments, and phonon degrees of freedom.

Model

Consider a quasi-two-dimensional (2D) layered model defined on a triangular lattice, where the electronic and local-moment degrees of freedom reside on alternating layers. The effective 2D Hamiltonian is given by (see ref. 39 for a microscopic derivation of H_{EME}),

$$H = H_{el} + H_S + H_K + H_{ph} + H_{el-ph} + H_{EME}, \quad [1a]$$

$$H_{el} = \sum_{\boldsymbol{k},\alpha} (\varepsilon_{\boldsymbol{k}} - \mu) p^\dagger_{\boldsymbol{k}\alpha} p_{\boldsymbol{k}\alpha}, \quad [1b]$$

$$H_S = J_H \sum_{\langle i,j \rangle} \boldsymbol{S}_i \cdot \boldsymbol{S}_j, \quad [1c]$$

$$H_K = J_K \sum_i p^\dagger_{i\alpha} (\boldsymbol{S}_i \cdot \boldsymbol{\sigma}_{\alpha\beta}) p_{i\beta}, \quad [1d]$$

$$H_{ph} = \sum_{\ell = I_a, I_o, O} \sum_{\boldsymbol{q}} \left(\frac{|\pi^{(\ell)}_{\boldsymbol{q}}|^2}{2M} + \frac{M\omega^2_{\ell,\boldsymbol{q}}}{2} |\varphi^{(\ell)}_{\boldsymbol{q}}|^2 \right), \quad [1e]$$

$$H_{el-ph} = \sum_{i,\sigma} \left(\alpha_a \nabla \varphi^{(I_a)}_i p^\dagger_{i\sigma} p_{i\sigma} + \alpha_o \varphi^{(I_o)}_i p^\dagger_{i\sigma} p_{i\sigma} \right), \quad [1f]$$

$$H_{EME} = \tilde{\alpha} \sum_i \varphi^{(O)}_i p^\dagger_{i\alpha} (\boldsymbol{S}_i \cdot \boldsymbol{\sigma}_{\alpha\beta}) p_{i\beta}. \quad [1g]$$

Here, $p^\dagger_{\boldsymbol{k}\sigma}$, $p_{\boldsymbol{k}\sigma}$ denote the Pd-electron creation and annihilation operators with momentum $\boldsymbol{k}$ and spin $\sigma = \pm 1/2$. The electronic dispersion is given by $\varepsilon_{\boldsymbol{k}}$, and μ is the chemical potential; experiments in $PdCrO_2$ indicate that the Pd-electronic structure is well captured using first- and second-neighbor hoppings and the conduction band, dominantly of Pd character, is very close to half-filling (23, 28). The local moments, $\boldsymbol{S}_i$, interact mutually via nearest-neighbor antiferromagnetic Heisenberg exchange ($J_H > 0$), and with the Pd-electron spin-density via a Kondo exchange ($J_K > 0$), respectively. The Cr-electrons form $S = \frac{3}{2}$ local moments (28). Finally, we include three phonon fields, $\varphi^{(\ell)}$ with $\ell = I_a, I_o, O$, corresponding to in-plane acoustic (I_a), in-plane optical (I_o), and out-of-plane (O) lattice vibrations, respectively. We set the mass, M, to be equal for these modes for simplicity. The in-plane modes $I_{a,o}$ couple to the p-electron density with strengths $\alpha_{a,o}$, respectively, while the out-of-plane mode, O, couples to the "interlayer" Kondo interaction with EME strength, $\tilde{\alpha}$. We set the lattice constant $a = 1$, unless stated otherwise. Importantly, we include couplings to both in-plane acoustic and optical modes to account for the full T-dependence of ρ_{ab} in the absence of magnetism (i.e., in $PdCoO_2$) (29). Henceforth, we neglect the weak momentum dependence and the form factors associated with the different interaction terms in the quasi-two-dimensional setting to simplify our discussion (28). We will restore these additional complexities when considering out-of-plane transport for reasons to be made clear below.

Let us begin by considering the simpler case where the optical modes are Einstein phonons, with $\omega_{I_o,\boldsymbol{q}} = \omega_0$ and

$\omega_{O,\boldsymbol{q}} = \widetilde{\omega}_0$, while for the acoustic mode $\omega_{I_a,\boldsymbol{q}} = cq$, with a corresponding Debye frequency ω_D. The experimental regime of interest corresponds to $\{\widetilde{\omega}_0, J_H\} \lesssim T \ll \varepsilon_F$, where ε_F is the Fermi energy for the Pd-electrons. Moreover, we shall consider the limit where $J_H \gg \{\widetilde{\alpha}\sqrt{\hbar/M\widetilde{\omega}_0},\ J_K\}$ and thereby ignore the feedback of both electrons and phonons on the properties of the local moments. In recent work (40), some of us analyzed the properties of a subset of the terms $(H_{el} + H_S + H_K)$ in Eq. **1a** at leading order in a small J_K by approximating the local moments as $O(3)$ vectors, but capturing their complex precessional dynamics using the Landau–Lifshitz equations (41–48). While this leads to an interesting frequency dependence and momentum-dependent cross-overs in the electronic self-energy, the temperature dependence can be understood entirely based on a high-temperature expansion with uncorrelated local moments. The present manuscript will treat the local moments on the same footing but include the additional interaction effects due to $(H_{ph} + H_{el-ph} + H_{EME})$.

Results for Intermediate-Scale Transport

We will analyze electrical transport for the model defined above within the framework of the traditional Landau–Boltzmann paradigm (8). This is justified based on the magnitude of the resistivity being much smaller than the characteristic scale of ha_B/e^2 ($a_B \equiv$ Bohr radius) and $k_F\ell_{mfp} \gg 1$ over the entire temperature range of interest (ℓ_{mfp} being the mean free path) (23). Moreover, there is direct experimental evidence for the value of the dimensionless Kondo-coupling being small, based on recent photoemission experiments (28).

Considering the full H, we have multiple sources of scattering for the electrons. Within Boltzmann theory, the total transport scattering rate satisfies Matthiessen's rule (8):

$$\frac{1}{\tau_{tr}} = \frac{1}{\tau_{el-ph}} + \frac{1}{\tau_K} + \frac{1}{\tau_{EME}}, \qquad [2]$$

and the in-plane resistivity is given by $\rho_{ab} = m/(ne^2\tau_{tr})$, where m is the effective mass and n is the electron density (39). Experiments with controlled amounts of irradiation shift the overall resistivity curves by a constant (and relatedly, the residual resistivity), without affecting the slope in the T-linear regime (31). We start by describing the electron–phonon contribution, $1/\tau_{el-ph} \equiv 1/\tau_{el-ph,a} + 1/\tau_{el-ph,o}$. Previous works have obtained $1/\tau_{el-ph}$ for $PdCoO_2$ and highlighted the importance of a high-frequency optical mode (which is not entirely in the equipartition regime at $T \lesssim \omega_0$) for the observed superlinear-scaling of $\rho_{ab}(T)$ (29, 58). We have fully reproduced these results for $PdCoO_2$ based on the same procedure (39) within our 2D model of the Fermi surface; see Fig. 2. In $PdCrO_2$, the scattering of electrons off the local moments due to the bare Kondo interaction, $1/\tau_K$, can lead to a sublinear T-dependent contribution to ρ_{ab} at temperatures $T \gtrsim J_H$, before saturating to the T-independent value (40) (see $\rho_K = m/(ne^2\tau_K)$ in the *Inset* of Fig. 2).

We now turn to the important role of the EME term in $PdCrO_2$. For $\widetilde{\omega}_0 \gtrsim J_H$, we find that τ_{EME}^{-1} follows closely the temperature dependence of the scattering rate of electrons interacting with an optical mode of frequency $\widetilde{\omega}_0$ with a modified dimensionless coupling,

$$\lambda_{EME} = \frac{\nu_0\widetilde{\alpha}^2}{M\widetilde{\omega}_0^2} S(S+1). \qquad [3]$$

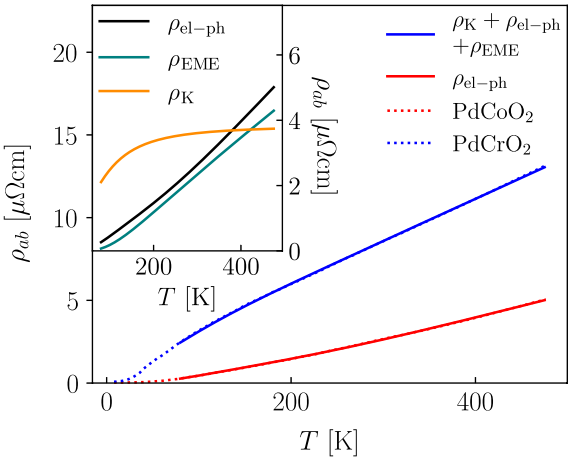

Fig. 2. Comparison of T-dependence of in-plane resistivity between experiments (23) (dotted lines) and theoretical model in Eq. **1a** (solid lines). The only free parameters in the fits are the phonon frequencies and bare el-ph and EME couplings. All other parameters are fixed; see refs. 28 and 39. For the phonon data, we have used $\omega_D = 29$ meV, $\omega_0 = 120$ meV, $\widetilde{\omega}_0 = 40$ meV, $\lambda_{el-ph,a} = 0.04$, $\lambda_{el-ph,o} = 0.02$, $\lambda_{EME} = 0.05$ and $S = 3/2$.

Here, ν_0 is the electronic density of states at the Fermi level, and scattering off the (spin−S) local-moment fluctuations via the EME interaction leads to the additional factor of $[S(S+1)]$ (39). Ignoring the constant offset, $1/\tau_K$ at $T \gg J_H$, we find that

$$\frac{1}{\tau_{tr}} \approx \frac{2\pi}{\hbar}\left(\lambda_{el-ph,a} + \lambda_{el-ph,o} + \lambda_{EME}\right) T, \quad T \gtrsim \omega_0, \qquad [4]$$

where the dimensionless coefficients are given by

$$\lambda_{el-ph,o} = \frac{\nu_0\alpha_o^2}{M\omega_0^2}, \quad \lambda_{el-ph,a} = \frac{\nu_0\alpha_a^2}{Mc^2}. \qquad [5]$$

Consequently, at the highest temperatures, the effect of the EME term considered in this work is to enhance the slope (A) of a T-linear resistivity, $\rho_{ab} - \rho_0 = AT$. This constitutes our first important result.

Importantly, even if the bare EME coupling is weak relative to the electron-acoustic phonon coupling (i.e., $\widetilde{\alpha}/\alpha_a \ll 1$), the dimensionless coupling λ_{EME} is not necessarily small compared to $\lambda_{el-ph,a}$. Furthermore, if the out-of-plane phonon is soft ($\widetilde{\omega}_0/\omega_D \ll \widetilde{\alpha}/\alpha_a$), the presence of the EME interaction can dramatically reduce the onset of T–linear resistivity to $\mathcal{O}(\widetilde{\omega}_0)$.

Assembling all of the above ingredients, we can now reproduce the resistivity in $PdCrO_2$, including the effect of the EME term; see Fig. 2. Note that the scattering rates due to the electron–phonon interaction in $PdCoO_2$ (58, 59) and Kondo coupling in $PdCrO_2$ (28) are fixed by previous experiments, which leaves two independent parameters in our theory—λ_{EME} and $\widetilde{\omega}_0$ [J_H is also fixed (28)]. We determine these parameters by fitting the excess resistivity $\Delta\rho$ in Fig. 1B to the analytical form of τ_{EME}^{-1} (39). The values obtained by this procedure are consistent with the characteristic out-of-plane lattice vibration frequency being naturally softer than the in-plane one, $\omega_0 \gtrsim \widetilde{\omega}_0 \gtrsim J_H$; however, we note that our theory extends beyond this regime. The resulting contribution to the resistivity, ρ_{EME}, is shown in the *Inset* of Fig. 2. Overall, the prominent T-linear resistivity at intermediate T stems from i) the EME scattering rate and ii) the combined sublinear and superlinear contributions of ρ_K and ρ_{el-ph}, respectively (39). It is worth noting that the T-linear behavior in Eq. **4** applies when all phonon modes are

in their equipartition regime. For $PdCrO_2$, this corresponds to $T \sim \mathcal{O}(1{,}000)$ K due to the large value of ω_0 and is hence not directly related to the behavior presented in Fig. 2.

Role of Acoustic Phonons

Our discussion thus far has focused on the simplified limit of an EME coupling to optical phonons. Let us now analyze the effects of an EME coupling to an acoustic phonon. For $H_{\rm ph}$ in Eq. **1e**, this amounts to replacing $\widetilde{\omega}_0^2 \left(\widetilde{\varphi}_q^{(O)}\right)^2 \rightarrow \widetilde{\omega}_{\boldsymbol{q}}^2 \left(\widetilde{\varphi}_q^{(O)}\right)^2$, where $\widetilde{\omega}_{\boldsymbol{q}} = \widetilde{c}q$ in the limit of small q. Similarly, for $H_{\rm EME}$ in Eq. **1g**, this amounts to replacing $\boldsymbol{\varphi}_i^{(O)} \rightarrow \nabla \boldsymbol{\varphi}_i^{(O)}$. Note that, in practice, the out-of-plane vibrations that couple the layers are at a finite wavevector, namely, $\omega_{\boldsymbol{q}} \approx \sqrt{\widetilde{c}^2 q_x^2 + \widetilde{c}^2 q_y^2 + \widetilde{c}_z^2 q_{z,0}^2}$ in the limit where $\widetilde{c}_z q_{z,0} \ll T$. It is worth noting that unlike the conventional electron–phonon interaction, where scattering is mainly small-angle up to the BG temperature, the EME term induces large-angle scattering even at low T due to large momentum transfer to the local moments, which serve as a "bath." If the spin structure factor exhibits nontrivial correlations in the Brillouin zone (i.e., the spin-correlation length is finite with remnants of Bragg-like peaks), the intermediate-scale transport behavior is controlled by the Pd-electron Fermi-surface geometry. However, when the spin-correlation length is short, $1/\tau_{\rm EME}$ shows two distinct regimes (39). For $T \gtrsim \widetilde{T}_{\rm BG} \equiv 2\widetilde{c}k_F$, the Bloch-Grüneisen temperature, the result reduces to the case of optical phonons, $1/\tau_{\rm EME} = 2\pi\lambda_{\rm EME} T$ with $\lambda_{\rm EME} = \frac{\nu_0 \widetilde{\alpha}^2}{M\widetilde{c}^2} S(S+1)$. On the other hand, for $J_{\rm H} \lesssim T \lesssim \widetilde{T}_{\rm BG}$, we encounter an unexpected $1/\tau_{\rm EME} = 2\pi\lambda_{\rm EME} T^2/\widetilde{T}_{\rm BG}$, instead of the usual $\sim T^4$ regime in two-dimensions for the phase-space reasons introduced above. Interestingly, this is an example of a T^2 "quasi-elastic" scattering due to the EME term (instead of the usual T^2 due to Umklapp scattering).

Effect of c-Axis Strain on In-Plane Transport

Given that the proposed EME interaction in $PdCrO_2$ originates from fluctuations of the (interlayer) Kondo coupling, applying c-axis pressure is expected to enhance the slope of the T-linear resistivity for the following reason. The bare EME coupling is controlled in part by the Kondo scale, $\widetilde{\alpha} \propto t_{cp}^2/U$, where t_{cp} is the interplane hybridization between the Pd and Cr-electrons and U is the on-site Coulomb repulsion for Cr-electrons (28, 39). Upon applying c-axis strain, the interlayer distance reduces, thereby increasing t_{cp}, which is exponentially sensitive to the deformation; the stiffening of the out-of-plane phonons is at best algebraic. Therefore, the dimensionless EME coupling, $\lambda_{\rm EME} \propto t_{cp}^4/(U\widetilde{\omega}_0)^2$ is expected to show a significant increase, along with an enhancement of the Kondo coupling which affects the constant shift in the resistivity at high T. The predicted form of the in-plane transport is depicted in the *Inset* of Fig. 3*B* for a range of $c-$axis strain (ε_{zz}) for bare microscopic parameters as chosen in Fig. 2.

Out-of-Plane Transport

The electrical resistivity along the c-axis provides a direct window into the interlayer nature of the magnetic interactions, which we have absorbed so far in the effective 2D model. We consider the leading contributions to the c-axis conductivity within linear-response theory, which is given by

$$\sigma_c = \sigma_{\rm coh} + \sigma_{\rm K} + \sigma_{\rm EME}, \qquad [6]$$

where $\sigma_{\rm coh}$ arises from the "coherent" channel due to interlayer p to p hoppings (t_{pp}), and $\sigma_{\rm K}$, $\sigma_{\rm EME}$ represent the "incoherent" channels due to interlayer spin-assisted and spin-phonon-assisted contributions, respectively (39). For simplicity, we ignore the contribution due to an interlayer "incoherent" phonon-assisted hopping not involving the local moments; such a term does not affect our results at a qualitative level. The leading-order Feynman diagrams corresponding to each of these contributions are depicted in Fig. 3*A*. We have $\sigma_{\rm coh} = e^2(n/m)_c \tau_{\rm tr}$, where $(n/m)_c$ is related to the c-axis dispersion and $\tau_{\rm tr}$ is given by Eq. **2**; the detailed expressions for the incoherent channels appear in (39).

The coherent channel dominates σ_c up to temperatures $T \lesssim T_* \sim 10^3$ K [determined by the condition $\sigma_{\rm coh}(T_*) \approx \sigma_{\rm EME}(T_*)$ (39)], such that, in this T-regime, σ_c and σ_{ab} follow the same T-scaling as they share the same transport lifetime. The contribution of the incoherent channels becomes significant at temperatures $T \gtrsim T_*$, where, due to the weak c-axis dispersion, their temperature dependence is determined by the T-scaling of the current vertices, rather than the transport lifetime. In particular, for $T \gtrsim \omega_D, \widetilde{\omega}_0$, while $\sigma_{\rm coh} \sim 1/T$ as in the in-plane case, $\sigma_{\rm K}$ is independent of T and $\sigma_{\rm EME} \propto T$. As a result, the c-axis resistivity becomes sublinear at sufficiently high temperatures, as depicted in Fig. 3*B*.

The interplay between the different conduction mechanisms has signatures in the behavior under c-axis pressure. The in-plane conductivity is expected to decrease with c-axis compression since the EME scattering is enhanced (because it is proportional to the interplane hopping strength). In contrast, the coherent part of the c-axis conductivity increases, as a result of the enhanced interlayer hopping (39). Interestingly, this increase in $\sigma_{\rm coh}$ is associated solely with the el–ph scattering term. The contributions to $\sigma_{\rm coh}$ from the Kondo and EME terms are proportional to t_{pp}^2/t_{cp}^4 (39);

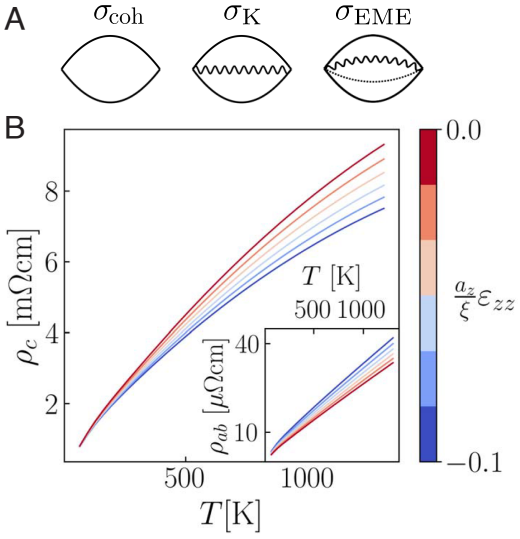

Fig. 3. (*A*) The Feynman diagrams contributing at leading order to the c-axis conductivity, σ_c (Eq. **6**), where solid, wiggly, and dashed lines denote electrons, spins, and phonons, respectively. (*B*) c-axis resistivity as a function of T for different (compressive) c-axis strain ε_{ZZ} (in units of ξ/a_Z, where ξ is the characteristic decay length of the hopping integral and a_Z is the $\hat{z}$ lattice constant). *Inset*: In-plane resistivity as a function of T under c-axis strain ε_{ZZ}.

assuming that $t_{pp} \propto t_{cp}^2$, the ratio t_{pp}^2/t_{cp}^4 is unchanged by c-axis strain. Similarly, the incoherent parts of the conductivity increase with compression. However, they do so slightly in excess of σ_{coh}, which in turn reduces the cross-over scale T_*, as manifested by the increase in curvature at intermediate temperatures with increasing compression; see Fig. 3*B* (39). There are measurements of the *c*-axis resistivity in the literature (60, 61), but the reported values are inconsistent with each other. The reason for this discrepancy is currently unclear. To resolve these issues, more accurate measurements are needed, using, for example, the techniques described in ref. 62.

Outlook

Our conjectured magneto-elastic mechanism for the enhanced T-linear resistivity in $PdCrO_2$ relies on quasi-elastic scattering, where the phonons are in the equipartition regime. There is experimental evidence for the Lorenz ratio satisfying the Wiedemann–Franz law in the T-linear regime (31), which is consistent with our mechanism. Interestingly, the extracted transport scattering rate in the same regime of T-linear resistivity is Planckian with $C \approx 0.9$ (31). Within our model and in the quasi-elastic regime, this is not indicative of any fundamental principle, such as a bound associated with an inelastic scattering rate. It is, however, far from obvious why the scattering rate turns out to be Planckian.

A natural future direction is to study the effects of the EME term at low temperature. In particular, the magneto-elastic coupling might be evident in the electronic spectral function. Signatures of phonon drag observed in $PdCoO_2$ (58) are expected to be suppressed in $PdCrO_2$ due to EME-induced large-angle scattering of phonons off magnetic moments (25). Pronounced magnetic correlations may also lead to a generalized Kohn anomaly (63) associated with phonon softening at the AFM wavevectors. A detailed understanding of the low-temperature properties of this interesting system remains an open problem.

Data, Materials, and Software Availability. All study data are included in the article and/or *SI Appendix*. Previously published data were used for this work (31).

ACKNOWLEDGMENTS. J.F.M.-V. and D.C. acknowledge the hospitality of the Weizmann Institute of Science, where this work was completed. J.F.M.-V. and D.C. thank A. McRoberts and R. Moessner for an earlier related collaboration and insightful discussions. D.C. thanks P. Coleman, J. Ruhman, and T. Senthil for useful discussions. J.F.M.-V. and D.C. are supported in part by a CAREER grant from the NSF to D.C. (DMR-2237522). D.C. and E.B. acknowledge the support provided by the Aspen Center for Physics where this collaboration was initiated, which is supported by NSF grant PHY-1607611. Research in Dresden benefits from the environment provided by the DFG Cluster of Excellence ct.qmat (EXC 2147, project ID 390858940).

Author affiliations: [a]Department of Physics, Cornell University, Ithaca, NY 14853; [b]Department of Condensed Matter Physics, Weizmann Institute of Science, Rehovot 76100, Israel; [c]Max Planck Institute for Chemical Physics of Solids, 01187 Dresden, Germany; and [d]Scottish Universities Physics Alliance, School of Physics & Astronomy, University of St. Andrews, St. Andrews KY16 9SS, United Kingdom

1. D. Chowdhury, A. Georges, O. Parcollet, S. Sachdev, Sachdev-Ye-Kitaev models and beyond: Window into non-Fermi liquids. *Rev. Mod. Phys.* **94**, 035004 (2022).
2. C. M. Varma, Colloquium: Linear in temperature resistivity and associated mysteries including high temperature superconductivity. *Rev. Mod. Phys.* **92**, 031001 (2020).
3. J. A. N. Bruin, H. Sakai, R. S. Perry, A. P. Mackenzie, Similarity of scattering rates in metals showing T-linear resistivity. *Science* **339**, 804–807 (2013).
4. S. A. Hartnoll, A. P. Mackenzie, Colloquium: Planckian dissipation in metals. *Rev. Mod. Phys.* **94**, 041002 (2022).
5. Y. Cao *et al.*, Strange metal in magic-angle graphene with near Planckian dissipation. *Phys. Rev. Lett.* **124**, 076801 (2020).
6. A. Legros *et al.*, Universal T-linear resistivity and Planckian dissipation in overdoped cuprates. *Nat. Phys.* **15**, 142–147 (2019).
7. G. Grissonnanche *et al.*, Linear-in temperature resistivity from an isotropic Planckian scattering rate. *Nature* **595**, 667–672 (2021).
8. J. M. Ziman, *Electrons and Phonons: The Theory of Transport Phenomena in Solids* (Oxford University Press, 1960).
9. H. Takagi *et al.*, Systematic evolution of temperature-dependent resistivity in $La_{2-x}Sr_xCuO_4$. *Phys. Rev. Lett.* **69**, 2975–2978 (1992).
10. N. E. Hussey *et al.*, Dichotomy in the T-linear resistivity in hole-doped cuprates. *Philos. Trans. R. Soc. A: Math., Phys. Eng. Sci.* **369**, 1626–1639 (2011).
11. N. Doiron-Leyraud *et al.*, Correlation between linear resistivity and T_c in the Bechgaard salts and the pnictide superconductor $Ba(Fe_{1-x}Co_x)_2As_2$. *Phys. Rev. B* **80**, 214531 (2009).
12. T. Shibauchi, A. Carrington, Y. Matsuda, A quantum critical point lying beneath the superconducting dome in iron pnictides. *Annu. Rev. Condens. Matter Phys.* **5**, 113–135 (2014).
13. P. B. Allen *et al.*, Transport properties, thermodynamic properties, and electronic structure of srruo$_3$. *Phys. Rev. B* **53**, 4393–4398 (1996).
14. L. Klein *et al.*, Anomalous spin scattering effects in the badly metallic itinerant ferromagnet $SrRuO_3$. *Phys. Rev. Lett.* **77**, 2774–2777 (1996).
15. N. E. Hussey *et al.*, Normal-state magnetoresistance of Sr_2RuO_4. *Phys. Rev. B* **57**, 5505–5511 (1998).
16. M. Schneider *et al.*, Low-energy electronic properties of clean $CaRuO_3$: Elusive Landau quasiparticles. *Phys. Rev. Lett.* **112**, 206403 (2014).
17. A. W. Rost *et al.*, Thermodynamics of phase formation in the quantum critical metal $Sr_3Ru_2O_7$. *Proc. Natl. Acad. Sci. U.S.A.* **108**, 16549–16553 (2011).
18. G. R. Stewart, Non-Fermi-liquid behavior in *d*- and *f*-electron metals. *Rev. Mod. Phys.* **73**, 797–855 (2001).
19. A. Jaoui *et al.*, Quantum critical behaviour in magic-angle twisted bilayer graphene. *Nat. Phys.* **18**, 633–638 (2022).
20. E. H. Hwang, S. Das Sarma, Linear-in-*T* resistivity in dilute metals: A Fermi liquid perspective. *Phys. Rev. B* **99**, 085105 (2019).
21. S. Das Sarma, F. Wu, Strange metallicity of Moiré twisted bilayer graphene. *Phys. Rev. Res.* **4**, 033061 (2022).
22. S. A. Hartnoll, A. P. Mackenzie, Colloquium: Planckian dissipation in metals. *Rev. Mod. Phys.* **94**, 041002 (2022).
23. C. W. Hicks *et al.*, Quantum oscillations and magnetic reconstruction in the delafossite $PdCrO_2$. *Phys. Rev. B* **92**, 014425 (2015).
24. V. Eyert, R. Frésard, A. Maignan, On the metallic conductivity of the delafossites $PdCoO_2$ and $PtCoO_2$. *Chem. Mater.* **20**, 2370–2373 (2008).
25. H. Takatsu, H. Yoshizawa, S. Yonezawa, Y. Maeno, Critical behavior of the metallic triangular-lattice Heisenberg antiferromagnet $PdCrO_2$. *Phys. Rev. B* **79**, 104424 (2009).
26. K. P. Ong, J. Zhang, J. S. Tse, P. Wu, Origin of anisotropy and metallic behavior in delafossite $PdCoO_2$. *Phys. Rev. B* **81**, 115120 (2010).
27. A. P. Mackenzie, The properties of ultrapure delafossite metals. *Rep. Prog. Phys.* **80**, 032501 (2017).
28. V. Sunko *et al.*, Probing spin correlations using angle-resolved photoemission in a coupled metallic/Mott insulator system. *Sci. Adv.* **6**, eaaz0611 (2020).
29. H. Takatsu *et al.*, Roles of high-frequency optical phonons in the physical properties of the conductive delafossite $PdCoO_2$. *J. Phys. Soc. Jpn.* **76**, 104701 (2007).
30. A. Glamazda *et al.*, Collective excitations in the metallic triangular antiferromagnet $PdCrO_2$. *Phys. Rev. B* **90**, 045122 (2014).
31. E. Zhakina *et al.*, Investigation of Planckian behavior in a high-conductivity oxide: $PdCrO_2$. arXiv [Preprint] (2023). http://arxiv.org/abs/2301.10631 (Accessed 27 January 2023).
32. H. Takatsu *et al.*, Magnetic structure of the conductive triangular-lattice antiferromagnet $PdCrO_2$. *Phys. Rev. B* **89**, 104408 (2014).
33. R. Daou, R. Frésard, V. Eyert, S. Hébert, A. Maignan, Unconventional aspects of electronic transport in delafossite oxides. *Sci. Technol. Adv. Mater.* **18**, 919–938 (2017).
34. H. J. Noh *et al.*, Anisotropic electric conductivity of delafossite $PdCoO_2$ studied by angle-resolved photoemission spectroscopy. *Phys. Rev. Lett.* **102**, 256404 (2009).
35. H. J. Noh *et al.*, Direct observation of localized spin antiferromagnetic transition in $PdCrO_2$ by angle-resolved photoemission spectroscopy. *Sci. Rep.* **4**, 3680 (2014).
36. V. Sunko *et al.*, Maximal Rashba-like spin splitting via kinetic-energy-coupled inversion-symmetry breaking. *Nature* **549**, 492–496 (2017).
37. H. Takatsu, Y. Maeno, Single crystal growth of the metallic triangular-lattice antiferromagnet $PdCrO_2$. *J. Cryst. Growth* **312**, 3461–3465 (2010).
38. M. D. Le *et al.*, Magnetic interactions in $PdCrO_2$ and their effects on its magnetic structure. *Phys. Rev. B* **98**, 024429 (2018).
39. See *SI Appendix* (2023).
40. A. J. McRoberts, J. F. Mendez-Valderrama, R. Moessner, D. Chowdhury, Intermediate-scale theory for electrons coupled to frustrated local moments. *Phys. Rev. B* **107**, L020402 (2023).
41. A. Keren, Dynamical simulation of spins on Kagomé and square lattices. *Phys. Rev. Lett.* **72**, 3254–3257 (1994).
42. R. Moessner, J. T. Chalker, Properties of a classical spin liquid: The Heisenberg pyrochlore antiferromagnet. *Phys. Rev. Lett.* **80**, 2929–2932 (1998).
43. R. Moessner, J. T. Chalker, Low-temperature properties of classical geometrically frustrated antiferromagnets. *Phys. Rev. B* **58**, 12049–12062 (1998).
44. P. H. Conlon, J. T. Chalker, Spin dynamics in pyrochlore Heisenberg antiferromagnets. *Phys. Rev. Lett.* **102**, 237206 (2009).
45. A. M. Samarakoon *et al.*, Comprehensive study of the dynamics of a classical Kitaev spin liquid. *Phys. Rev. B* **96**, 134408 (2017).

46. X. Bai *et al*., Magnetic excitations of the classical spin liquid $MgCr_2O_4$. *Phys. Rev. Lett.* **122**, 097201 (2019).
47. S. Zhang, H. J. Changlani, K. W. Plumb, O. Tchernyshyov, R. Moessner, Dynamical structure factor of the three-dimensional quantum spin liquid candidate $NaCaNi_2F_7$. *Phys. Rev. Lett.* **122**, 167203 (2019).
48. O. Franke, D. Călugăru, A. Nunnenkamp, J. Knolle, Thermal spin dynamics of Kitaev magnets–Scattering continua and magnetic field induced phases within a stochastic semiclassical approach. *Phys. Rev. B* **106**, 174428 (2022).
49. D. M. Kennes *et al*., Moiré heterostructures as a condensed-matter quantum simulator. *Nat. Phys.* **17**, 155–163 (2021).
50. K. F. Mak, J. Shan, Semiconductor Moiré materials. *Nat. Nanotechnol.* **17**, 686–695 (2022).
51. T. Li *et al*., Continuous Mott transition in semiconductor Moiré superlattices. *Nature* **597**, 350–354 (2021).
52. A. Ghiotto *et al*., Quantum criticality in twisted transition metal dichalcogenides. *Nature* **597**, 345–349 (2021).
53. A. Kumar, N. C. Hu, A. H. MacDonald, A. C. Potter, Gate-tunable heavy fermion quantum criticality in a Moiré Kondo lattice. *Phys. Rev. B* **106**, L041116 (2022).
54. A. Dalal, J. Ruhman, Orbitally selective Mott phase in electron-doped twisted transition metal-dichalcogenides: A possible realization of the Kondo lattice model. *Phys. Rev. Res.* **3**, 043173 (2021).
55. W. Zhao *et al*., Gate-tunable heavy fermions in a Moiré Kondo lattice. *Nature* **616**, 61–65 (2023). https://doi.org/10.1038/s41586-023-05800-7.
56. V. Vaňo *et al*., Artificial heavy fermions in a van der Waals heterostructure. *Nature* **599**, 582–586 (2021).
57. E. Persky *et al*., Magnetic memory and spontaneous vortices in a van der Waals superconductor. *Nature* **607**, 692–696 (2022).
58. C. W. Hicks *et al*., Quantum oscillations and high carrier mobility in the delafossite $PdCoO_2$. *Phys. Rev. Lett.* **109**, 116401 (2012).
59. H. Takatsu *et al*., Roles of high-frequency optical phonons in the physical properties of the conductive delafossite $PdCoO_2$. *J. Phys. Soc. Jpn.* **76**, 104701 (2007).
60. H. Takatsu, S. Yonezawa, C. Michioka, K. Yoshimura, Y. Maeno, Anisotropy in the magnetization and resistivity of the metallic triangular-lattice magnet $PdCrO_2$. *J. Phys: Conf. Ser.* **200**, 012198 (2010).
61. S. Ghannadzadeh *et al*., Simultaneous loss of interlayer coherence and long-range magnetism in quasi-two-dimensional $PdCrO_2$. *Nat. Commun.* **8**, 15001 (2017).
62. C. Putzke *et al*., *h*/*e* oscillations in interlayer transport of delafossites. *Science* **368**, 1234–1238 (2020).
63. W. Kohn, Image of the Fermi surface in the vibration spectrum of a metal. *Phys. Rev. Lett.* **2**, 393–394 (1959).